High-Fidelity CFD Verification Workshop 2024: Mesh Motion

Nathan A. Wukie*
Air Force Research Laboratory, Wright-Patterson AFB, United States

Krzysztof Fidkowski†
University of Michigan, Ann Arbor, MI, USA

Per-Olof Persson‡
University of California, Berkeley, Berkeley, CA, United States
Lawrence Berkeley National Laboratory, Berkeley, Berkeley, CA, United States

Z.J. Wang§
University of Kansas, Lawrence, KS, USA

Mesh motion test cases have been part of the High-Fidelity (previously High-Order) CFD Workshops since their inception in 2012 and continue in the next iteration, the High-Fidelity CFD Verification Workshop in 2024. Activities from the most-recent workshop (2022) helped multiple groups identify bugs, and yielded significantly improved agreement between participant results compared against previous workshop iterations. The present work evolves the test suite in preparation for the 2024 workshop. Specifically, the test suite targets volume scaling, breaks problem symmetries, and proposes a study on convergence of spatial and temporal errors and their impact on long-time stability. This paper details the evolution of the test suite and serves as a reference document leading up to and after the 2024 workshop.

Nomenclature

$\boldsymbol{u}$	Fluid state vector
ρ	Density
v_i	i-th component of velocity
E	Stagnation/total energy
M	Mach number
γ	Ratio of specific heats
W	Work
I	Impulse
$\vec{F}$	Force vector
$\vec{\tau}$	Torque vector
$\vec{v}_0$	Pivot velocity
$\vec{\omega}_0$	Angular velocity about pivot

*Research Engineer, Multidisciplinary Science & Technology Center, Air Force Research Laboratory, AIAA Senior Member.
†Professor, Department of Aerospace Engineering, University of Michigan, AIAA Associate Fellow.
‡Professor, Department of Mathematics, University of California, Berkeley
Faculty Scientist, Mathematics Group, Lawrence Berkeley National Laboratory, AIAA Senior Member.
§Spahr Professor, Department of Aerospace Engineering, University of Kansas, AIAA Fellow.

American Institute of Aeronautics and Astronautics

m Fluid mass
e_m Mass conservation error
h Height
θ Angular position
α Prescribed-motion function
β Prescribed-rotation function
f_g Deformation function
A_i Amplitudes of motion

I. Introduction

Fluid problems with moving or deforming domains are found in many important aerospace applications. Fluid-structure interaction, turbomachinery, store separation, and rotor-craft simulations are just a small subset of problems where the prediction of fluid phenomena on moving domains is very important. As a part of the High-Fidelity CFD Verification Workshop, previously known as the High-Order Workshop [1], we seek to provide a Mesh Motion suite of problems for the purpose of supporting code verification activities and to resolving outstanding technical challenges (e.g. data-set agreement, observed rates-of-convergence, long-time stability).

The Mesh Motion test suite is aimed at testing the accuracy of high-order flow solvers for problems with moving and deforming domains. The most recent iteration of this test suite included both moving cylinder and moving airfoil test cases [2]. Successes from the most recent workshop yielded greatly improved agreement in results for the moving cylinder test case. In the present work as a part of the 2024 High-Fidelity CFD Verification Workshop committee, we seek to evolve the test suite with the following objectives: to target volume scaling terms, to break problem symmetries, and to study the convergence of spatial and temporal errors and their impact on long-time stability. In the following sections, the moving cylinder and airfoil test cases are presented along with their extensions for the next workshop. This manuscript serves as the reference document to be utilized by participants in the Mesh Motion test suite for the 2024 High-Fidelity CFD Verification Workshop.

II. Flow in a cylinder

A. Geometry

The reference geometry for this problem is a circular cylinder for which several types of motion are prescribed. The center of motion coincides with the geometric center of the cylinder, and the fluid domain of interest is the cylinder interior volume. Figure 1 shows a diagram of the problem geometry and the fluid domain.

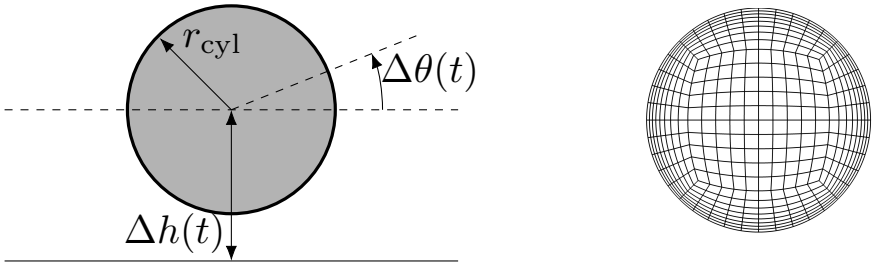

(a) Geometry diagram. **(b) Fluid domain.**

Figure 1: Cylinder problem description.

B. Extension summary

For the 2022 workshop, four prescribed motions were defined that corresponded to translation (Motion 1), rotation (Motion 2), constant-volume deformation (Motion 3), and a fourth motion defined as a composite of the first three (Motion 4). The past motions are detailed in the 2022 pre-workshop reference document

by Persson et al.[2]. Building on the lessons learned in the 2022 workshop, the cylinder test case has been extended with three main areas of study. These are:

1. **Symmetry breaking:** One problem with 2022 cylinder motions was that they possessed too much symmetry in space and time. This lead to certain integrated quantities being zero. We have modified the prescribed motions and time horizon to eliminate these symmetries, making cancellation of errors less likely and increasing the amount of data suitable for comparison.

2. **Non-unit geometry mapping Jacobian:** Another drawback of the 2022 cylinder motions is that the prescribed motions all had unit Jacobian determinant, g. This determinant pervades the equations of mesh motion, particularly in the arbitrary Lagrangian Eulerian transformations. A unit value for g thus limits the ability of a test case to identify implementation errors in the equations, including domain-interior and boundary treatments. We therefore have created a motion for the cylinder case in which $g \neq 1$ in the domain and on the boundary.

3. **The geometric conservation law and stability:** An often contentious topic in simulations of mesh motion is that of the geometric conservation law, which pertains to the ability of a numerical scheme to remain conservative in the presence of mesh motion. Whereas all finite-dimensional schemes introduce numerical error, discrete conservation in fluid dynamics problems is desirable for various reasons, including correct shock capturing. However, not all mesh motion schemes or implementations satisfy this property, and although fixes are available, subtle conservation errors can still persist, e.g. when using insufficiently-accurate quadrature rules [3]. Just as other numerical errors, these conservation errors decrease with mesh and time-step refinement, and hence their effect on the the cylinder cases, with short time horizons, was likely minor. In longer simulations, however, the impact of even small conservation errors may be more significant. A study on the effect of conservation errors as well as their long-time behavior and impact has been added.

C. Cylinder test cases

Two cylinder test cases are defined. Cylinder Case 1 is a short-time version of the 2022 Cylinder Motion-4, extended to include non-unit geometry mapping Jacobian. Wall boundary conditions will be used except for free-stream preservation tests relevant to the geometric conservation law, in which full-state boundaries will also be simulated. Cylinder Case 2 is a long-time study designed to measure the buildup of any errors associated with not satisfying the geometric conservation law.

Relevant constants for all motions are listed in Table 1. A_θ is a rotation amplitude, A_a is an amplification factor for the deformation of a circle into an ellipse, A_g is a volume deformation amplitude, and r_{cyl} is the initial radius of the cylinder wall for all motions. The transformation of the cylinder deforming into an ellipse

r_{cyl}	0.5
A_θ	π
A_a	1.5
A_g	0.15

Table 1: Cylinder motion constants.

such that the interior area remains constant during deformation is facilitated by the function

$$\psi(t) = 1 + (A_a - 1)\alpha(t) \tag{1}$$

which varies from 1 to A_a over $t = [0, 2]$, where $\alpha(t)$ is a time-activation function that is defined differently for each test case in the sections below. Next, a parameterized function η is defined as

$$\eta(\lambda, \omega, \tau) = \sin\left(\omega\lambda + \tau\left(1 - \cos\left(\omega\lambda\right)\right)\right) \tag{2}$$

which is designed to break spatial and temporal symmetries due to the fact that the integral of η over a period ω does not equal 0 for appropriate values of τ. The parameter λ represents the independent variable

(e.g. t or θ) whereas ω and τ represent the function frequency and shape characteristics. A subsequent function f_g is defined here to prescribe a deformation that ensures non-unit geometry mapping Jacobians ($g \neq 1$), while utilizing the η function to break spatial and temporal symmetries. This is given as

$$f_g(t, r_0, \theta_0) = \left(16r_0^4 + \frac{t^6}{t^6 + 0.01}\eta(t, 10, 0.7)\left(\cos\left(32\pi r_0^4\right) - 1\right)\right)\eta(\theta_0, 1, 0.7) \tag{3}$$

which was designed with the following properties in mind:

1. Initial prescribed deformation on the cylinder boundary $r_0 = 0.5$ at time $t = 0$, but the boundary deformation is not time-varying. In this way, non-trivial ($g \neq 1$) deformations exist on the wall boundary, yet the static nature of the deformation function on the wall ensures the physical problem is not modified; allowing data to be compared against prior workshop results.

2. Symmetry-breaking spatial perturbation $\eta(\theta_0, 1, 0.7)$.

3. Symmetry-breaking temporal perturbation $\eta(t, 10, 0.7)$.

4. Smooth start-up rapidly reaching an asymptotically periodic region around $t = 1$ via window function $t^6/(t^6 + 0.01)$.

The prescribed deformation takes the form of a perturbation in θ as

$$\theta_g(t, r_0, \theta_0) = \theta_0 + A_g f_g(t, r_0, \theta_0) \tag{4}$$

A composite motion (translation, rotation, deformation) is then formed by representing primitive motions as transformation matrices and composing them by matrix multiplication. Note, translation is not a linear transformation in (x, y)-space. However, translation can be accommodated by augmenting the transformation to $(x, y, 1)$-space. In contrast to the previous workshop motion where the primitive motions were operating on (x_0, y_0), the new motion operates on the deformed coordinates $(r_0\cos(\theta_g), r_0\sin(\theta_g))$. The prescribed motion is composed as

$$\begin{bmatrix} x \\ y \\ 1 \end{bmatrix} = \begin{bmatrix} 1 & 0 & 0 \\ 0 & 1 & \alpha(t) \\ 0 & 0 & 1 \end{bmatrix} \begin{bmatrix} \cos(A_\theta\alpha(t)) & -\sin(A_\theta\alpha(t)) & 0 \\ \sin(A_\theta\alpha(t)) & \cos(A_\theta\alpha(t)) & 0 \\ 0 & 0 & 1 \end{bmatrix} \begin{bmatrix} \psi(t) & 0 & 0 \\ 0 & \frac{1}{\psi(t)} & 0 \\ 0 & 0 & 1 \end{bmatrix} \begin{bmatrix} r_0\cos\left(\theta_g(t)\right) \\ r_0\sin\left(\theta_g(t)\right) \\ 1 \end{bmatrix} \tag{5}$$

1. Cylinder Case 1: short-time composite with deformation extension

The motion for Cylinder Case 1 is defined as a composite of three primitive motions; including translation, rotation, and deformation with the addition of the deformation function (f_g) described above. The time-activation function $\alpha(t)$ for this case is given as

$$\alpha(t) = t^3\left(8 - 3t\right)/16 \tag{6}$$

which varies from 0 to 1 on the interval $t = [0, 2]$. Case 1 shall be run from $t = 0$ until $t = 1$. The intent of this case in the test suite is to break any intrinsic symmetries in the flow field that may cause symmetric error contributions to cancel each other out; causing certain implementation errors to pass a test undetected. Figure 2 shows an example of the short-time problem along with the determinant of the Jacobian mapping g. Figure 2a portrays a notional initial mesh. Note, that the motion includes a deformation at $t = 0$, which is shown in Figure 2b and notable in Figure 2e. The final time $t = 1$ is also shown in Figures 2c and 2f.

The complexity of the new cylinder motion introduces significant opportunities for implementation error related to the prescribed motion. The motion, velocities, and spatial derivatives related to the motion may be required (depending on the numerical method and implementation approach). To reduce the opportunity for implementation errors the organizers will provide Python, C, and Fortran functions for the Cylinder prescribed motion and its spatial and temporal derivatives. These functions will be hosted on the workshop website `highfidelitycfdverificationworkshop.github.io` under the Mesh Motion test suite.

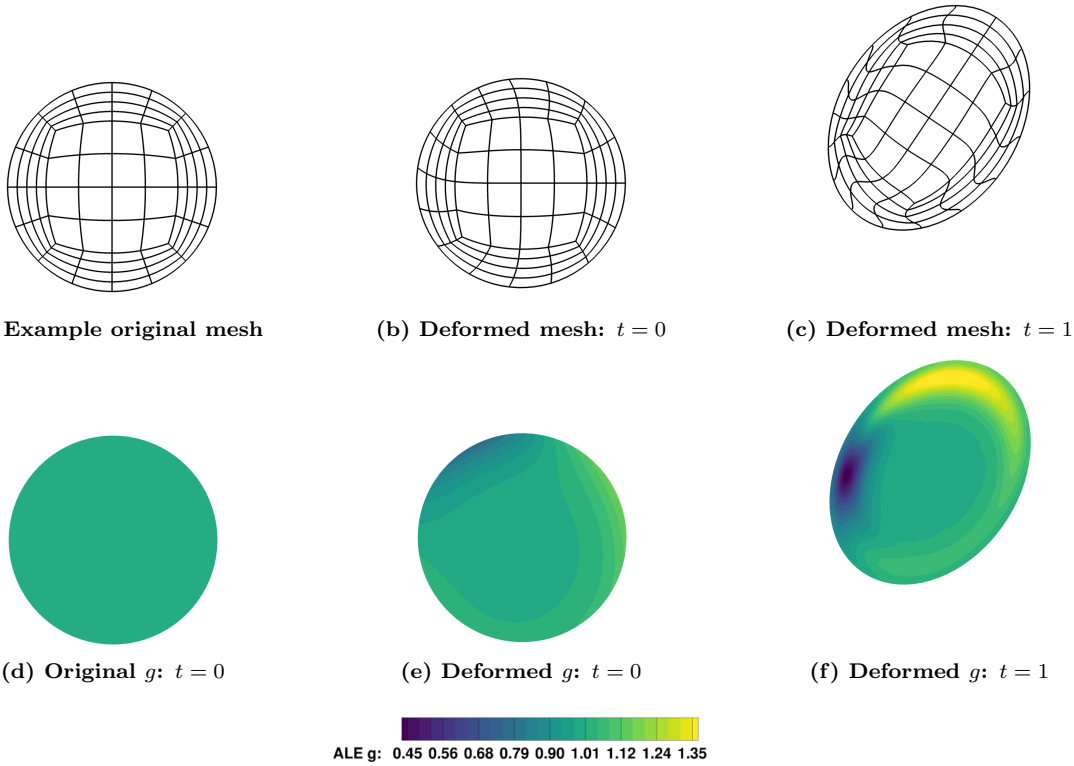

(a) Example original mesh **(b) Deformed mesh:** $t = 0$ **(c) Deformed mesh:** $t = 1$

(d) Original g**:** $t = 0$ **(e) Deformed** g**:** $t = 0$ **(f) Deformed** g**:** $t = 1$

Figure 2: Cylinder Case 1: short-time version of a composite motion extended for $g \neq 1$

2. Cylinder Case 2: long-time study of conservation

The motion for Cylinder Case 2 has the same form as that of the composite motion for Cylinder Case 1, but with a different $\alpha(t)$ function. To allow for long-time simulations, $\alpha(t)$ will be a ramped sine:

$$\alpha(t) = \alpha_{\max} \sin(\omega_\alpha t) \frac{t^6}{t^6 + t_{\text{ref}}^6}, \tag{7}$$

where $\alpha_{\max} = 0.3$, $\omega_\alpha = 6$, and $t_{\text{ref}} = 1$. The purpose of the second term in the equation is to start the sinusoidal motion slowly and smoothly at $t = 0$. Case 2 shall be run for a longer time, from $t = 0$ until $t = 40$. Running this motion for a long time will test to what extent mass conservation errors, which may arise in formulations that do not explicitly enforce the geometric conservation law [3], build up in the solution.

D. Governing equations and flow conditions

The governing equations for this problem are 2D compressible Navier-Stokes with a constant ratio of specific heats equal to 1.4, a Prandtl number of 0.72 and a constant viscosity. For cases running with wall boundaries, the cylinder interior is prescribed with a no-slip, adiabatic wall boundary condition. The initial condition at time $t = 0$ is given by the conserved-variable state vector

$$\boldsymbol{u}|_{t_0} = [\rho, \rho v_1, \rho v_2, \rho E]|_{t_0} = [1, 0, 0, 50.]$$

For this test suite, a single Reynolds number $Re = 1000$ should be simulated. The reference velocity is chosen to be 1.0 and the reference length scale is the cylinder diameter, $d = 2r_{\text{cyl}} = 1.0$.

III. Heaving-pitching airfoil

These cases involve a NACA 0012 airfoil undergoing a smooth flapping-type motion, starting from rest at zero angle of attack and ending at a one chord length higher position at the end of the motion at time T. Two motions are considered at one Reynolds number, Re = 1000, based on the chord length.

A. Geometry

The geometry consists of a NACA 0012 airfoil with chord length $c = 1$, with geometry modified to give zero trailing edge thickness:

$$y(x) = \pm 0.6(0.2969\sqrt{x} - 0.1260x - 0.3516x^2 + 0.2843x^3 - 0.1036x^4), \quad x \in [0, 1].$$

The far-field boundary should be located at least 100 chord-lengths away from the airfoil.

B. Motion

The airfoil undergoes a smooth upward motion of one chord length for the duration of $T = 2$ time units, by heaving and pitching about a point located at the airfoil 1/3 chord location (see figure). We consider two different motions with different properties. The underlying functions for the motions are given here:

$$\alpha(t) = t^3 (8 - 3t) /16$$
$$\beta(t) = -t^6 + 6t^5 - 12t^4 + 8t^3$$

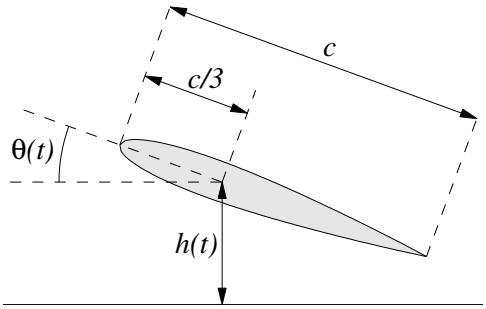

Table 2 presents the two motion descriptions in terms of vertical and angular displacements, where $B_\theta = 80\pi/180$.

	Motion 1	Motion 2
$\Delta h(t)$	$\alpha(t)$	$\alpha(t)$
$\Delta\theta(t)$	0	$B_\theta \cdot \beta(t)$

Table 2: Heaving-pitching airfoil prescribed-motion test cases, $t \in [0, 2]$

C. Governing equations and flow conditions

The governing equations for this problem are the 2D compressible Navier-Stokes equations with a constant ratio of specific heats equal to 1.4, a Prandtl number of 0.72 and a constant viscosity. Two boundary conditions are imposed: far-field characteristic conditions at the outer domain and no-slip adiabatic wall condition on the moving airfoil.

The free-stream Mach number is horizontal and two Mach number cases are requested $M_\infty = [0.01, 0.2]$. The Mach number $M = 0.01$ case has been added to approximate incompressibility and facilitate comparison between participants (both for compressible and incompressible methods). The Reynolds number based on the chord of the airfoil is $\mathrm{Re} = 1000$. The initial condition at time $t = 0$ is the steady-state solution for the initial position $h = 0$, $\theta = 0$. To simplify post-processing, we assume convenient units in which the airfoil chord is $c = 1$ and the free-stream density and speed are unity, so that the free-stream conservative state vector is

$$[\rho, \rho u, \rho v, \rho E] = \left[1,\ 1,\ 0,\ 0.5{+}1/[M^2\gamma(\gamma - 1)]\right].$$

D. Example results

A subset of results are presented here to give insight into the behavior for the heaving-pitching airfoil problem. Figure 3 shows contours of vorticity for both prescribed motions, where a variety of vortical flow structures are present in the flow field. Additionally, Figure 4 shows time-histories for output quantities for each motion.

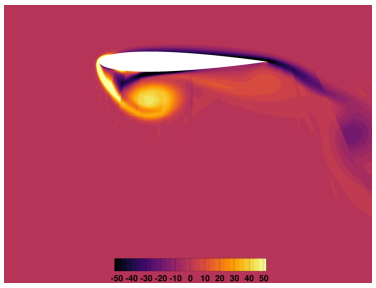

(a) Motion 1: Heaving @ $t = 1.5$

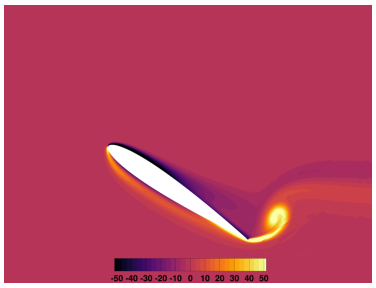

(b) Motion 2: Heaving + Pitching @ $t = 0.5$

Figure 3: Heaving-pitching airfoil contours of vorticity for motions at intermediate-time, $M = 0.2$

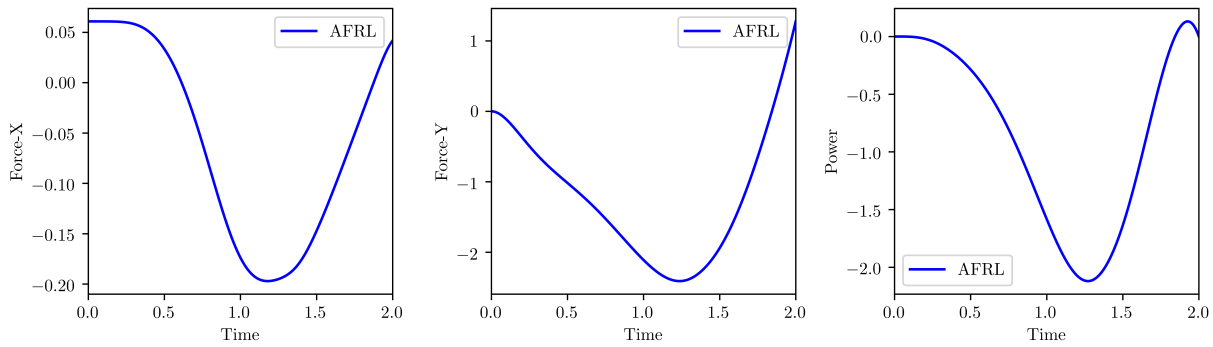

(a) Motion 1 (translation)

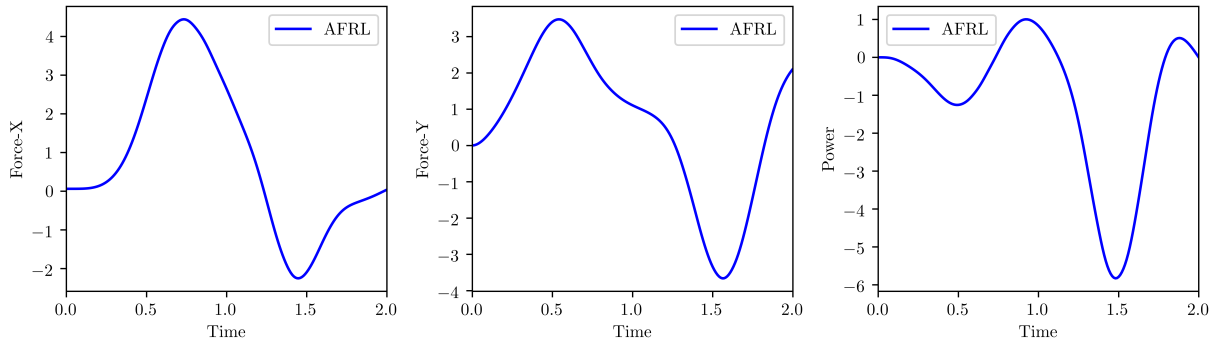

(b) Motion 2 (translation + rotation)

Figure 4: Force and power histories for airfoil test cases, $M = 0.2$

IV. Outputs

A. Work

The first output is the work (energy) that the fluid exerts on the surface of the cylinder during the motion, which can be written as

$$W = \int_0^T \vec{F}(t) \cdot \vec{v}_0 dt + \int_0^T \vec{\tau}(t) \cdot \vec{\omega}_0 dt = \int_0^T F_y(t)\dot{h}(t)dt + \int_0^T \tau_z(t)\dot{\theta}(t)dt \tag{8}$$

Here, $\vec{F}(t) = [F_x(t), F_y(t)]$ is the force imparted by the fluid on the surface, $\vec{\tau}(t) = [0, 0, \tau_z(t)]$ is the torque imparted by the fluid on the surface about the reference pivot point (cylinder center), $\vec{v}_0 = \dot{h}(t)$ is the velocity of the pivot point, and $\vec{\omega}_0 = [0, 0, \dot{\theta}]$ is the angular velocity of the cylinder about the pivot point. Note, that this output can be equivalently computed as

$$W = \int_0^T \int_{\text{surface}} \vec{v}_G(t) \cdot \vec{f}_{\text{surf}}(t)\, ds\, dt \tag{9}$$

where $\vec{v}_G(t)$ is the velocity of the surface and $\vec{f}_{\text{surf}}(t)$ is the surface stress vector.

B. Impulse

The second output is the vertical impulse from the fluid onto the surface during the motion,

$$I = \int_0^T F_y(t)dt \tag{10}$$

C. Mass conservation

For the *Flow In A Cylinder* test case, the fluid mass should remain constant for all time. Two error metrics for mass conservation are requested. The first mass error metric is the error in total mass conservation accumulated over time, which shall be computed as

$$e_{m,1} = \sqrt{\frac{1}{T}\int_0^T (m_t - m_0)^2\, dt}, \tag{11}$$

where m_0 is the initial fluid mass integrated discretely at time $t = 0$ and m_t is the fluid mass integrated discretely at a given time t. The fluid mass shall be computed as

$$m_t = \int_{\text{volume}} \rho(t) dV. \tag{12}$$

The second error metric for mass conservation measures pointwise mass errors,

$$e_{m,2} = \frac{1}{T}\int_0^T \int_{\text{volume}} |\rho(t) - \rho_{\text{ref}}(t)|\, dV dt, \tag{13}$$

where $\rho_{\text{ref}}(t)$ is a reference density that could come from the initial condition for static cases with moving meshes, or from higher-fidelity calculations on finer spatial and temporal discretizations.

V. Requirements

The data requested for this test suite are summarized here. Partial data for a subset of test cases will also be accepted for making meaningful comparisons.

1. Perform the indicated simulation for the test cases. Report time-histories of integrands from temporal integrals in Eqns. 9-13 for each case, and perform a grid/timestep convergence study to get the values as accurate as possible. The time-histories requested are summarized in Eqns. 14-17. The organizers

will compute the temporal integrals and normalizations in Eqns. 9-13 from the submitted time-history data in order to construct data set comparisons.

Y-Force	$F_y(t)$	(14)
Work integrand	$\int_{\text{surface}} \vec{v}_G(t) \cdot \vec{f}_{\text{surf}}(t)\, ds$	(15)
Mass	$\int_{\text{volume}} \rho(t) dV$	(16)
Mass error	$\int_{\text{volume}} \lvert\rho(t) - \rho_{\text{ref}}(t)\rvert\, dV$	(17)

2. Record the converged output values and nDOFs in the discretization (spatial and temporal) and submit this data to the case organizers.

3. Describe in detail the mesh-motion formulation that was used to generate the results. This includes motion implementation, transformation equations, boundary treatment, and any underlying assumptions.

VI. Summary

This paper details the Mesh Motion test suite for the 2024 High-Fidelity CFD Verification Workshop. The objective of including this suite in the workshop is to identify implementation differences and common errors in high-fidelity fluid simulations on moving and deforming domains. Such simulations are increasingly of interest, particularly in problems with aeroelastic phenomena where fluid-structure interaction is of importance. Previous workshops worked to achieve consensus in results for a moving cylinder test case, which was successful. The present work extends the test suite to target a broader set of potential conditions (e.g. volume-scaling), an expanded set of test cases (e.g. long-time cylinder, low-mach airfoil), and issues related to accuracy and stability (e.g. geometric conservation law). This serves as a reference document for participants in the next High-Fidelity CFD Verification Workshop. Additional information may be found on the workshop website `highfidelitycfdverificationworkshop.github.io`.

References

[1] Wang, Z., Fidkowski, K., Abgrall, R., Bassi, F., Caraeni, D., Cary, A., Deconinck, H., Hartmann, R., Hillewaert, K., Huynh, H., Kroll, N., May, G., Persson, P.-O., van Leer, B., and Visbal, M., "High-Order CFD Methods: Current Status and Perspective," *International Journal for Numerical Methods in Fluids*, 2013. doi:10.1002/fld.3767.

[2] Persson, P.-O., Fidkowski, K., and Wukie, N. A., "High-Fidelity CFD Workshop 2022: Mesh Motion," *2021 AIAA SciTech Forum*, 2021. AIAA 2021-1551.

[3] Persson, P.-O., Bonet, J., and Peraire, J., "Discontinuous Galerkin solution of the Navier-Stokes equations on deformable domains," *Computational Methods in Applied Mechanics and Engineering*, Vol. 198, 2009, pp. 1585–1595.